Daytime vertical E × B drift velocities inferred from ground-based magnetometer observations at low latitudes

David Anderson and Adela Anghel

Cooperative Institute for Research in Environmental Sciences, University of Colorado and Space Environment Center, National Oceanic and Atmospheric Administration, Boulder, Colorado, USA

Jorge Chau and Oscar Veliz

Radio Observatorio de Jicamarca, Lima, Peru

[1]   The daytime equatorial electrojet is a narrow band of enhanced eastward current flowing in the $100-120$ km altitude region within $\pm 2°$ latitude of the dip equator. A unique way of determining the daytime strength of the electrojet is to observe the difference in the magnitudes of the horizontal (H) component between a magnetometer placed directly on the magnetic equator and one displaced $6°-9°$ away. The difference between these measured H values provides a direct measure of the daytime electrojet current and, in turn, the magnitude of the vertical E × B drift velocity in the F region ionosphere. This paper discusses a recent study where 27 months of magnetometer H component observations and daytime, vertical E × B drift velocities were obtained in the Peruvian longitude sector between August 2001 and December 2003. In order to establish the relationships between ΔH and E × B drift velocities for the 270 days of observations, three approaches were chosen: (1) a linear regression analysis, (2) a multiple regression approach, and (3) a neural network approach. The neural network method gives slightly lower RMS error values compared with the other two methods. The relationships for all three techniques are validated using an independent set of E × B drift observations from the Jicamarca incoherent scatter radar (ISR) located at Jicamarca, Peru. The techniques presented here will be incorporated into a recently developed, real-time Global Assimilation of Ionospheric Measurements (GAIM) model.   INDEX TERMS: 2400 Ionosphere; 2411 Ionosphere: Electric fields (2712); 2409 Ionosphere: Current systems (2708); 2415 Ionosphere: Equatorial ionosphere; KEYWORDS: ionosphere, electrodynamics, equatorial electrojet, magnetometer, neural network, space weather

1. Introduction

[2]   Rastogi and Klobuchar [1990] suggested and demonstrated that the strength of the daytime equatorial electrojet could be measured using two magnetometers, one situated on the magnetic equator and the other displaced by 6 to 9 degrees away. Using this technique they were able to infer whether the daytime vertical E × B drift velocity in the F region was large or small. They compared the difference in the Horizontal (H) component values between magnetometers at Trivandrum (8.5°N, 77.0°E., 0.5°S dip lat.) and Alibag (18.5°N, 72.9°E, 13.0°N dip lat.) with the observations of Total Electron Content (TEC) measured by a chain of polarimeters as a function of latitude and local time in the Indian subcontinent. It is well known that large upward E × B drift velocities produce the equatorial anomaly with crests in the peak electron density, Nmax, and TEC at ±15° dip latitude while the absence of E × B drift does not create the anomaly. They verified that a weak equatorial electrojet was accompanied by an absence in TEC crests, while a strong

electrojet (large ΔH values) was accompanied by observed daytime crests in TEC at ±15° dip latitude. They also found that measuring the day-to-day fluctuation in H at only one station − Trivandrum − was not a realistic measure of the strength of the equatorial electrojet. Anderson et al. [1992] subsequently carried out theoretical calculations of TEC as a function of local time and latitude and compared these with the Indian TEC observations. They found excellent agreement for both "weak" and "strong" electrojet days. Neither Rastogi and Klobuchar [1990] nor Anderson et al. [1992] presented a quantitative relationship between ΔH and E × B drift − only a qualitative one.

[3]   In a recent paper by Anderson et al. [2002] it was demonstrated that there exists quantitative relationships whereby the vertical E × B drift velocity in the equatorial F region can be estimated using ground-based magnetometer observations. Such quantitative relationships were developed for the South American sector, during the Solar Maximum period, $1998-1999$. This represented the first time such a unique relationship had been quantitatively
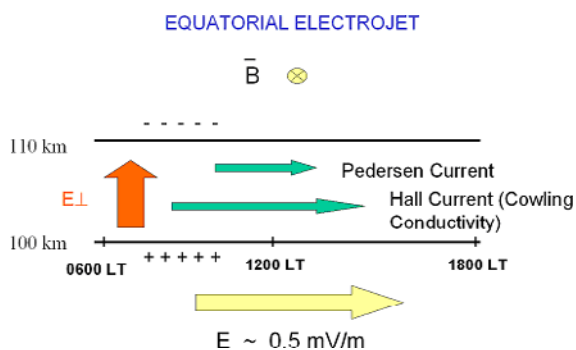
Figure 1. Schematic diagram of equatorial electrojet electric fields and current systems.

established. The Jicamarca Incoherent Scatter Radar (ISR) provided the daytime, vertical **E** × **B** drift velocities in conjunction with magnetometers at Canete and Piura in Peru. However, the data sets were only available for a total of 11 days between 1998 and 1999. The purpose of this paper is to quantitatively determine the relationships over a much longer period of time, using a significantly larger database of vertical **E** × **B** drift velocities and magnetometer observations.

[4] This paper (1) describes briefly the physics of electrodynamics of the equatorial electrojet, (2) describes the data sets that provide the vertical **E** × **B** drift velocities and the magnetometer observations, (3) Outlines the linear least squares method, the multiple regression technique and the neural network approach in developing the relationships, (4) validates the relationships by demonstrating how well the inferred daytime **E** × **B** drift velocities compare with actual measured drifts throughout the day, and (5) Summarizes a few of the scientific studies that can now be carried out knowing the day-to-day variability in the magnitude of **E** × **B** drift velocities and how these results have practical applications for Navigation and Communication system users.

[5] From a space weather perspective, being able to realistically specify the daytime vertical **E** × **B** drift velocities on a day-to-day basis, means that the low-latitude F region ionosphere can now be specified much more realistically since daytime, upward **E** × **B** drift is the primary transport mechanism that determines electron density profiles as a function of latitude and local time between ±20° dip latitude. A recently developed, theoretical, Global Assimilation of Ionospheric Measurements (GAIM) model [*Schunk et al.*, 2004] uses a Kalman Filter approach to assimilate all available, real-time ground-based and satellite observations of ionospheric parameters. The GAIM model requires that a realistic ionospheric representation be achieved before the assimilation process is applied. Being able to specify the low-latitude **E** × **B** drift velocities is an integral part of GAIM. The techniques that we have developed and present in this paper will be incorporated into the GAIM model that is currently being transitioned for operational status at the Air Force Weather Agency (AFWA) at Offutt AFB, Nebraska and the NOAA

Space Environment Center (SEC), Boulder, Colorado. In the future, running GAIM in real time at AFWA and SEC will provide DoD and Civilian Navigation and Communication System customers with an ionospheric specification and forecast capability that currently does not exist.

2. Low-Latitude Electrodynamics

[6] It is well known that the effect of neutral winds together with diurnal and semidiurnal tidal components in the atmosphere cause currents to flow in the 100 to 130 km altitude region. This is the so-called Sq (Solar quiet) wind dynamo current system in the E region. Resulting from this current system is an electrostatic field directed eastward from dawn to dusk at low latitudes. The strength of this electric field is about 0.5 mV/m and is responsible for the upward **E** × **B** drift velocities of ∼20 m/sec measured by the Jicamarca ISR. As a result of this electric field, within ±2° of the magnetic equator, an enhanced eastward current flows (between 100 and 110 km altitude) known as the equatorial electrojet (see *Richmond* [1989] and *Reddy* [1989] for in-depth reviews of the neutral wind dynamo and the equatorial electrojet, respectively).

[7] Figure 1 depicts the eastward electric field (yellow arrow), the consequent vertical electric field (red arrow) and the current systems that are associated with the electrojet. The view is to the North at the magnetic equator viewing the dayside region. If an eastward electric field exists and is perpendicular to B, then a Hall current is generated in the downward direction. Because of the particular geometry at the magnetic equator where magnetic field lines are horizontal, the Hall current, carried by upward moving electrons, quickly polarizes the ionospheric E layer so that an upward directed polarization electric field is produced. This electric field (red arrow) is about 5 to 10 times stronger than the eastward electric field (yellow arrow) that produced it. It is this vertical electric field that is responsible for the eastward equatorial electrojet current. This current produces the strong enhancement in the H component observed by magnetometers within ±5° of the magnetic equator.

[8] Figure 2 is a schematic plot of typical noontime magnetometer H component observations as a function of latitude. Note the 100 nanoTesla (nT) increase near the dip equator superimposed on the "global" Sq current magnetometer observations. When the H component observations from a magnetometer 6 to 9 degrees away from the magnetic equator are subtracted from the H component values measured by a magnetometer on the magnetic equator, the difference is only related to the electrojet contribution which, in turn, is directly related to the eastward electrostatic field that created the electrojet current. Carrying out this subtraction to provide a ΔH value is necessary in order to eliminate the Dst ring current component in H, resulting in a ΔH value that is only related to the ionospheric electrojet current and hence the east-west electric field. This eastward electric field might originate from the Sq Wind dynamo
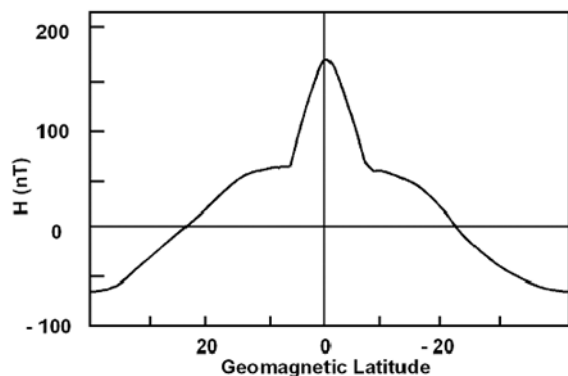
Figure 2. Schematic plot of typical noontime magnetometer H component observations as a function of latitude.

mechanism or could be associated with a penetration electric field from high latitudes, or both. It is emphasized that the electric field is ionospheric in origin and is not associated with the Dst "ring" currents, or the Tail currents.

3. Jicamarca Unattended Long-Term Ionosphere Atmosphere Radar (JULIA)

[9] The JULIA radar at Jicamarca, Peru provides the daytime, vertical E × B drift velocities that will be related to the ground-based magnetometer observations. The JULIA radar is a low-power 50 MHz coherent scatter system located at the Jicamarca Radar Observatory near Lima, Peru. The JULIA system is intended for uninterrupted and very cost effective observations of equatorial ionospheric field aligned irregularities (electrojet, spread F and 150 km echoes) and atmospheric irregularities (troposphere and lower stratosphere). Since its deployment in 1996, it has been used extensively in observing equatorial plasma density irregularities, particularly from the E and F regions [e.g., *Hysell et al.*, 1997; *Hysell and Burcham*, 1998; *Hysell and Burcham*, 2000] and

neutral atmospheric waves. In this study, JULIA observations are devoted to the daytime echo returns that occur near the 150 km altitude region.

[10] Echoes from 150 km altitude were first observed in the early 1960s [*Balsley*, 1964], however their existence is still puzzling [e.g., *Kudeki and Fawcett*, 1993; *Blanc et al.*, 1996; *Tsunoda and Ecklund*, 2000]. Nonetheless as it has been mentioned before, their Doppler velocities can be used to measure the zonal electric field in the equatorial ionosphere. *Kudeki and Fawcett* [1993] obtained a high correlation between the Doppler velocities from 150 km echoes and simultaneous ground magnetogram records made in Ancon. In addition, *Woodman and Villanueva* [1995] verified via incoherent scatter experiments that the 150 km echo phase velocities are indeed good estimates of F region vertical plasma drifts.

[11] As suggested by *Kudeki and Fawcett* [1993], these echoes can be detected with smaller systems (smaller antennas and/or less transmitted power) [e.g., *Kudeki et al.*, 1998; *Hysell et al.*, 1997]. The JULIA system is configured to excite two 30 kW peak power 50 MHz transmitters generating pulse lengths to about 15 μs with a 2% maximum duty cycle using the main Jicamarca antenna.

[12] Between August 2001 and December 2003, almost 270 days of 150 km echoes with the JULIA system were obtained using one half of the Jicamarca antenna for both transmission and reception, pointing perpendicular to B with good detectability. The Doppler estimates are obtained via a spectral estimation routine similar to the one applied by *Chau* [1998] to process echoes from the lower atmosphere.

[13] Given the intermittency of the 150 km echoes both in time and height, the velocities between the 135 and 167 km ranges have been averaged in order to decrease the statistical uncertainties of the echoes. Figure 3 displays the observed 150 km echo vertical drift velocities on 11 August 2001 between 10 and 16 LT.

4. Ground-based Magnetometer Observations

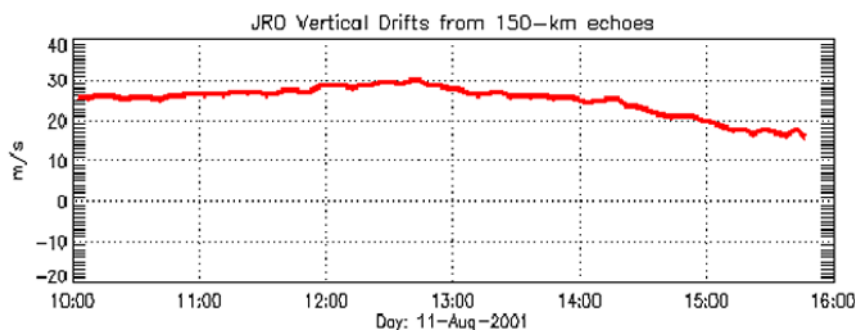[14] Two fluxgate magnetometers are operating currently at Jicamarca (11.92°S, 76.87°W) and Piura (5.18°S,

Figure 3. Observed vertical daytime E × B drift velocities on 11 August 2001 obtained from the JULIA 150 km echo returns (see text for details).
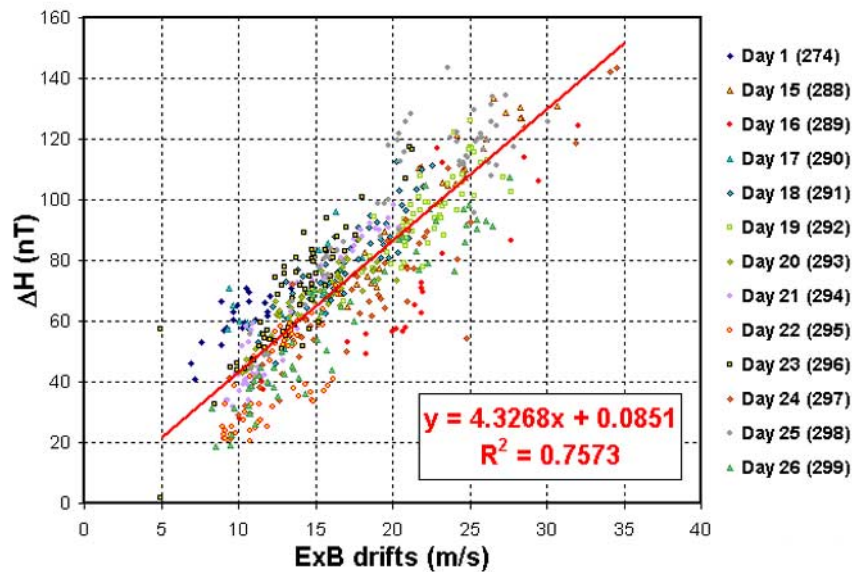
Figure 4. ΔH versus $\mathbf{E} \times \mathbf{B}$ drift values; linear, least squares straight line; and the days in October 2002 when the observations were made.

80.64°W). The instrument operating at Piura is a three-component linear fluxgate magnetometer donated by the Tromso University, Norway. Ten seconds and one minute mean values of H, D, and Z components are obtained with 1 nT resolution. The other magnetometer was installed at the Jicamarca Radio Observatory in October 1997. It is composed of a three ring core fluxgate high sensitive sensor. The three components H, D, Z are obtained every second with 0.1 nT resolution.

[15] As described by *Anderson et al.* [2002], for each of the magnetometer data sets at Jicamarca and Piura, the night-time baseline in H was first obtained for each day and then subtracted to give the daytime values. This produced daytime H component values at each of the stations for all of the days we will be considering. Both the JULIA daytime $\mathbf{E} \times \mathbf{B}$ drift velocities and the magnetometer H component observations for this study were available from August 2001 to December 2003.

5. Linear Least Squares Approach to Data Analysis

[16] Beginning in August 2001, and for each month, through December 2003 (except March and May 2002), the difference between the Jicamarca and Piura H component values, ΔH, and the observed JULIA vertical $\mathbf{E} \times \mathbf{B}$ drift velocity were plotted every 5 min between 10 and 16 LT. For each month, a linear, least squares relationship was assumed and the ΔH versus $\mathbf{E} \times \mathbf{B}$ drift velocity slope and intercept of the straight line were calculated. Figure 4 plots the ΔH versus $\mathbf{E} \times \mathbf{B}$ drift values, the regression line and the 13 days in October 2002 when the measurements were made. This same

analysis was carried out for each of the 27 months from August 2001 through December 2003, excluding March and May in 2002.

[17] Note that in October 2002 there were 13 days when the JULIA radar was observing vertical $\mathbf{E} \times \mathbf{B}$ drifts between 10 and 16 LT. For all of the 27 months there was an average of 10 days/month of JULIA observations that were used to determine the linear, least squares relationship. Figure 5 plots the ΔH versus $\mathbf{E} \times \mathbf{B}$ drift relationships when both values are positive for all 27 months, listing both the slopes and the intercepts for each month.

[18] We relate the monthly slope changes between August 2001 and December 2003, with the calculated monthly average of the F10.7 cm flux value. The rationale for choosing this relationship lies in the fact that ΔH is proportional to the equatorial electrojet current, which in turn is proportional to the conductivity times the eastward electric field, σE. Since the conductivity is directly related to NmE, the peak electron density of the daytime ionospheric E layer at an altitude around 120 km, and NmE is directly related to the solar flux of ionizing radiation, the conductivity is proportional to the solar flux of ionizing radiation plus other factors. An index for this ionizing radiation is the solar F10.7 cm flux value. These ΔH and NmE relationships were studied by *Richmond* [1973] who found that a 10% increase in NmE produced a 10% increase in ΔH. The monthly average F10.7 cm flux value is calculated for each of the days in the month when JULIA $\mathbf{E} \times \mathbf{B}$ drift data was available. We relate this to the monthly ΔH versus $\mathbf{E} \times \mathbf{B}$ drift velocity slope value. This relationship is displayed in Figure 6. Figure 6 implies that at solar minimum when
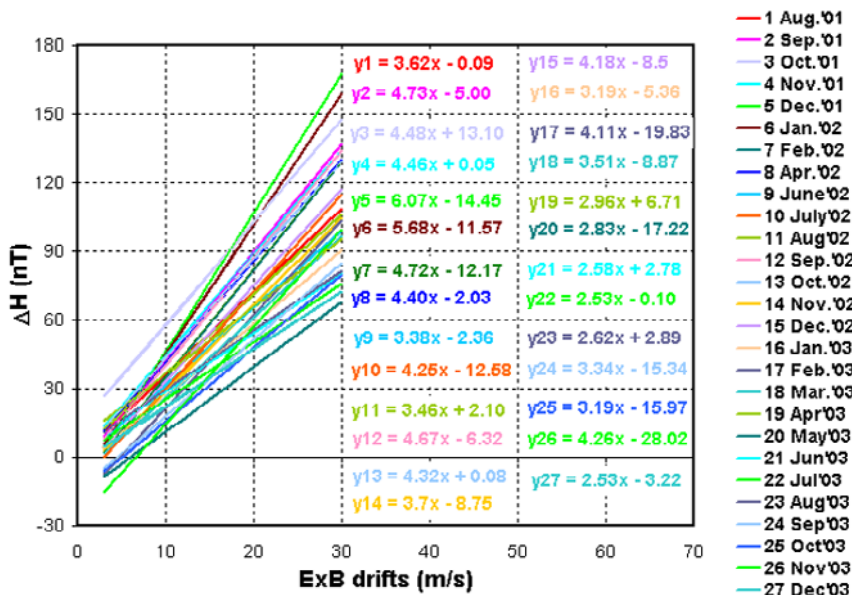
Figure 5. ΔH versus $E \times B$ drift velocity slopes and intercepts for all 27 months.

the F10.7 cm flux is ∼70 units, the ΔH versus $E \times B$ drift slope will be ∼1.4 nT/m/sec.

6. Multiple Regression Approach to Data Analysis (Least Squares Method (LSM))

[19] The monthly slopes calculated in the previous section give quantitative linear relationships between ΔH and $E \times B$ drifts that are specific for certain months. In the multiple regression approach, the purpose is to find a more general formula to estimate the $E \times B$ drift velocities. Having in view that there are some other input parameters that can improve the ΔH versus $E \times B$ drift linear relationship, the multiple regression technique [*Moore and McCabe*, 1993] has been considered. It is clear that the F10.7 cm flux value is an important parameter that has to be included beside ΔH in order to estimate the $E \times B$ drift velocities. We perform a multiple regression analysis for three cases presented in Table 1: (1) when the independent variable is only ΔH, (2) when the independent variables are ΔH and F10.7, and (3) when the independent variables are year, DOY (day of the year), F10.7, F10.7A, daily *Ap*, *Kp*, LT (local time) and ΔH.

[20] The regression parameters in all the three cases were calculated using the least squares method on the basis of data between August 2001 and September 2003, when Jicamarca 150 km observations and Jicamarca and Piura magnetometer measurements were available. The RMS error is defined by $SQRT[\Sigma(E \times B \ drift_{observed} - E \times B \ drift_{inferred})^2/N]$, where N is the number of 5 minute local time intervals for each day.

[21] The multiple regression technique is suitable when the relationship of the dependent variable ($E \times B$ drift velocity) to independent variables is linear. In the above cases the polynomial regression was also used to capture the nonlinear relationship between ΔH and $E \times B$ drift velocities. In general, if the exact nature of the nonlinearity is known, it can sometimes be compensated for by suitably transforming the independent variables. Unfortunately, in our case the exact nature of the nonlinearity is not known, and this is the reason why the neural network method has been considered.

7. Neural Network Approach to Data Analysis

[22] It is known that any problem that can be solved with traditional modeling or statistical methods can most likely be solved more effectively with a neural network. Neural networks are widely used in pattern recognition problems and in various artificial intelligence applications. In general, they are an attempt to model the behavior of a biological brain in a much simpler manner.
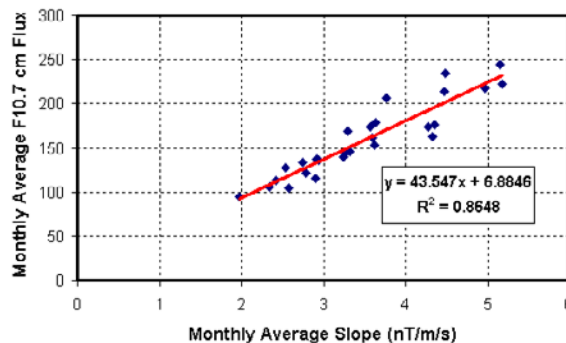

Figure 6. Monthly average F10.7 cm flux versus the monthly average slope (see text for details).

Table 1. Least Squares Method Formulas to Estimate Equatorial Daytime Vertical **E** × **B** Drift Velocities

E × B Drift	RMS Error, m/s
$5.2889 + 0.1947\Delta H + 0.0001\Delta H^2 - 0.0000021\Delta H^3$	3.79
$12.26 - 0.0454\,F10.7 + 0.1892\Delta H + 0.00028\Delta H^2 - 0.0000022\Delta H^3$	3.36
$-1989.51 + 1.002\text{year} - 0.00022\text{DOY} - 0.0222\,F10.7 - 0.0282\,F10.7A - 0.0229Ap\text{daily} + 0.0589Kp - 0.3661LT + 0.1865\Delta H + 0.00028\Delta H^2 - 0.0000023\Delta H^3$	3.21

[23] Multilayer feed-forward neural networks are a particular class of neural networks and have powerful function-approximation capabilities [*Masters*, 1993; *Haykin*, 1994]. A network consists of a set of processing elements called neurons that are logically arranged into two or more layers. There is an input layer and an output layer, each containing at least one neuron, and there are usually one or more hidden layers sandwiched between the input and output layers. Each neuron from the network has associated a nonlinear activation function except the neurons from the input layer. The layers are interconnected through a set of weights. Because of this distributed form of nonlinear processing, these structures are able to produce highly nonlinear mappings between inputs and outputs. If any of the nonlinearities are known in advance, a functional link network can be used to improve learning. These are powerful tools in modeling and identification of the nonlinear dynamical systems. They do not require us to choose a model and noise patterns are tolerated better than they are by most other methods. A network with one hidden layer can learn most of the mapping functions. However, a network having two hidden layers is a universal function approximator and it is needed to learn a function that is mostly continuous but has a few discontinuities. The learning and generalization capabilities of multilayer feed-forward neural networks are impressive. In general, few hidden neurons are required and with proper design of the network and training set, the training time is manageable. The regression can be interpreted as a neural network with one input and one output layer, and the neurons having a linear activation function, the identity function.

[24] A multilayer feed-forward neural network is trained in a supervised way in the sense that many training samples are collected to serve as exemplars and presented to the network. Each sample in this training set completely specifies all inputs, as well as the outputs that are desired when those inputs are presented. For training, a subset of the training data set is chosen and shown to the network. For each sample in this subset, the outputs from the network are compared with the desired outputs. After all the samples from the subset are shown to the network, the network's weights are adjusted according to the back-propagation algorithm, a gradient descent algorithm that minimizes the mean square error between the outputs produced by the network and the desired outputs. The network stores information within the weights on the connection links, therefore training consists in modifying the weights in order to bring the network closer to the desired outputs. In this way, during training, the hidden layers with nonlinear activation functions progressively extract more and more features from the input data. One pass through the subset of training samples, along with an updating of the network's weights, is called an epoch, and the number of samples in the subset is called the epoch size. In our case, the entire training set is used for each epoch, as this favors stability in convergence to the optimal weights.

[25] In this paper a multilayer feed-forward neural network has been considered in order to calculate the nonlinear relationship between E × B drift velocities and the 8 inputs to the network (year, DOY, F10.7, F10.7A, daily *Ap*, *Kp*, LT, and ΔH). For the training phase, 242 days of data between August 2001 and September 2003 were used. This makes 13,570 training samples with data between 10 and 16 LT. Networks with different architectures with one or two hidden layers and for different initial weights have been trained, over thousands of training epochs, but the best error value and training time were obtain with a network that has one hidden layer with 5 neurons, like the one in Figure 7. Figure 8 shows the error of our neural network for the training set as a function of the number of iterations of training done. The training phase was interrupted after 370 training epochs when the RMS error for
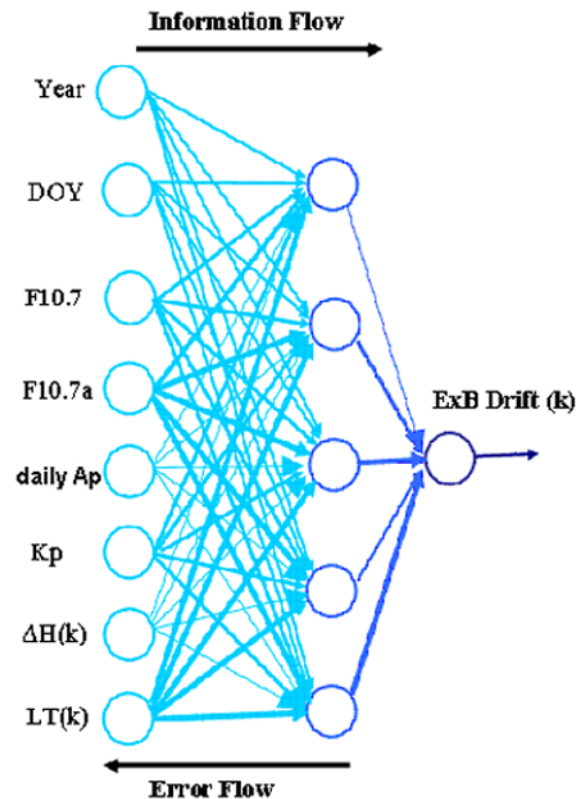

Figure 7. Neural network schematic.

Figure 8. Training error diagram.

the whole training set reached 2.9 m/sec. After 150 training epochs the error curve starts to flatten out, in other words, after that the network could not learn much more from the training set. This can be caused by the fact that there are some parameters that were not included as inputs but they might be crucial in reducing the training error. Another cause for a large training error can be attributed to the neural network itself, the way it was implemented and trained. Training algorithms, like the one used by our network, that minimize the mean square error across the training set don't pay sufficient attention to some particular cases if the error can be reduced by learning the most representative and frequent cases.

[26] In the following, the problem of identifying the most relevant inputs has been investigated using the regression and neural network techniques. A method related to stepwise discriminant analysis has been considered. The method consists in retraining a neural network individually for each input and the one that performs best is kept. This procedure is repeated by adding a second input. Inputs are added until no significant improvement is found. We considered six cases that are presented in Table 2. For the first two cases a network has been trained with only one input, ΔH, considered to be the most important input parameter. Then, for the third case LT has been added as input to the network. For case 4, daily Ap and Kp were added as inputs and for case 5, DOY and year. There is a significant improvement in the RMS error in case 6, when F10.7 and F10.7A were added as inputs. This means

that beside ΔH, F10.7 and F10.7A are other significant input parameters. The six cases are listed below with the RMS errors associated for each case and for each of the two methods used. It is emphasized that the important result shown in Table 2 is not a comparison between the neural network and multiple regression approaches, but a demonstration of the importance of input parameters and how different independent variables yield different RMS errors for both approaches. The next section provides a comparison of the approaches using an independent data set.

8. Validation of the Approaches

[27] Between April 2001 and November 2003, there were 38 days when the Jicamarca Incoherent Scatter Radar (ISR) in Peru was measuring the vertical **E** × **B** drift velocities. We have chosen these observations as our independent database in comparing the 3 approaches presented in this paper. Extracting the ISR **E** × **B** drift velocities between 10 and 16 LT for each of the 38 days gives 2254 samples to validate the realism of these relationships. Figure 9 displays the ISR observations (red line) on 17 April 2002 and on 25 September 2003, and compares the **E** × **B** drift velocities versus local time obtained from the 3 approaches. In each case the neural network approach (with 8 inputs) gives the lowest RMS error. Over the 38 days, the average RMS error for the multiple regression method is 4.59 m/sec and for the neural network approach is 4.21 m/sec.

9. Discussion and Summary

[28] The *Anderson et al.* [2002] paper first quantified the ΔH versus **E** × **B** drift velocity relationship but was limited to only 11 days of data between 1998 and 1999. In this paper, we have analyzed roughly 270 days between August 2001 and December 2003. The data sets have been analyzed using 3 different techniques: (1) linear, least squares method; (2) multiple regression approach; and (3) neural network approach. We find that the neural network approach gives slightly better results when comparing the RMS errors. Because the large data set covered so many consecutive months, it was possible to extract the F10.7 cm flux dependence, explicitly, as shown in Figure 6.

Table 2. RMS Errors Associated With Various Least Squares Method and Neural Network Approaches

| Least Squares Method (LSM) and Neural Network (NN) Approach	RMS Error, m/s
E × **B** (LSM) = $a_0 + a_1\Delta H$	3.82
E × **B** (NN) = 1 input (ΔH)	3.76
E × **B** (LSM) = $a_0 + a_1\Delta H + a_2\Delta H^2 + a_3\Delta H^3$	3.79
E × **B** (NN) = 1 input (ΔH)	3.76
E × **B** (LSM) = $a_0 + a_1\Delta H + a_2\Delta H^2 + a_3\Delta H^3 + a_4$LT	3.75
E × **B** (NN) = 2 inputs (ΔH, LT)	3.75
E × **B** (LSM) = $a_0 + a_1\Delta H + a_2\Delta H^2 + a_3\Delta H^3 + a_4Kp + a_5Ap + a_6$LT	3.68
E × **B** (NN) = 4 inputs (ΔH, LT, Ap, Kp)	3.67
E × **B** (LSM) = $a_0 + a_1\Delta H + a_2\Delta H^2 + a_3\Delta H^3 + a_4$DOY + $a_5$year + a_6LT	3.39
E × **B** (NN) = 4 inputs (ΔH, LT, year, DOY)	3.24
E × **B** (LSM) = $a_0 + a_1\Delta H + a_2\Delta H^2 + a_3\Delta H^3 + a_4$F10.7 + a_5F10.7a + a_6LT	3.25
E × **B** (NN) = 4 inputs (ΔH, LT, F10.7, F10.7A)	3.02
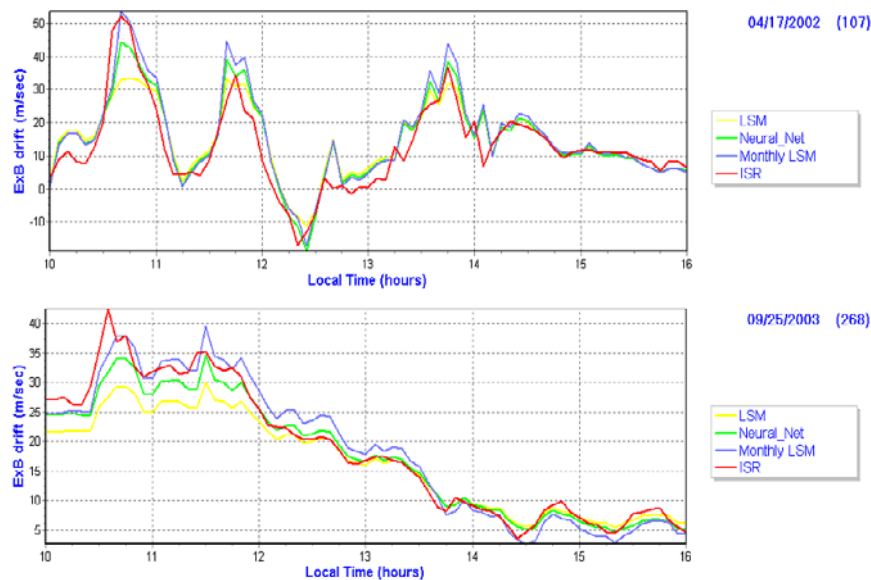
Figure 9. Comparison between the Jicamarca ISR observed **E** × **B** drifts and the three data analysis approaches for 17 April 2002 and 25 September 2003.

[29] An interesting question that needs to be answered is the role that E region, neutral tidal forcing plays in affecting the ΔH versus **E** × **B** drift relationships. *Richmond* [1973] demonstrated that a variation in the propagating diurnal tide affected the H component value away from the equator much more than the H component value at the magnetic equator. Referring to Figure 4, there are a few days in October 2002, days 16, 21 and 23, where the slope matches the monthly slope, but the intercepts are different. This could be a manifestation of the day-to-day variability in the diurnal and semidiurnal tides, that would affect the magnetometer at Piura more than the one at Jicamarca. Appropriate neutral wind observations and theoretical modeling efforts will be required to supply the answers.

[30] Another important area of study concerns the penetration of high-latitude electric fields to low latitudes. A number of theoretical studies [*Spiro et al.*, 1988; *Fejer and Scherliess*, 1995; *Peymirat et al.*, 2000] have investigated the "under shielding" and "over shielding" effects that allow the instantaneous penetration of high-latitude electric fields associated with geomagnetic storms and substorms to low latitudes. The sudden changes in vertical **E** × **B** drifts presented in Figure 9 are an example of such penetration events. The fact that the absolute magnitude of the drifts and their time dependence can now be monitored on a routine basis means that the output of theoretical models that predict the penetration effects can be validated for specific high-latitude storm and substorm periods. In a recent paper by *Kelley et al.* [2003], the Jicamarca- observed eastward, daytime electric field was compared with the time variation in the Interplanetary Electric Field (IEF) on 17 April 2002. A remarkable, one-to-one time variation was observed with the IEF being about 15 times greater than the low-latitude, eastward electric field. It is expected that for steady state IEF conditions, the corresponding daytime, vertical **E** × **B** drift velocities will exhibit a "quiet" Sq dynamo type pattern. The intriguing question is how the low-latitude daytime eastward electric field "evolves" from "quiet" to "disturbed" conditions as the IEF "evolves" from steady state to highly fluctuating conditions.

[31] Being able to specify realistic vertical **E** × **B** drift velocities as inputs to theoretical, time-dependent ionospheric models will allow realistic low-latitude electron and ion density distributions to be calculated and compared with observed ionospheric parameters. This is especially important in understanding the low-latitude ionospheric response to large geomagnetic storms such as the Halloween storms in October 2003.

[32] We have derived the ΔH versus **E** × **B** drift relationships for the Peruvian longitude sector and the question that remains to be answered is whether the same relationship holds at other longitude sectors. It can be argued that since the climatological, daytime **E** × **B** drift velocities are similar at all longitudes [*Scherliess and Fejer*, 1999], then the ratio of E/B is equivalent at all longitudes ($\mathbf{E} \times \mathbf{B}/B^2 = E/B$). This implies that the ΔH versus **E** × **B** drift relationship at other longitude sectors should be similar to the relationship in the Peruvian longitude sector if the same Sq dynamo wind systems exist and the penetration of high-latitude electric fields to low latitudes is absent.

[33] Finally, there are practical applications for the results and techniques we have presented. In the equatorial region of the Earth's ionosphere, strong, daytime upward **E** × **B** drift velocities produce very large crests in peak electron densities and Total Electron Content (TEC) values at ±16 to 18° dip latitude. All single frequency GPS receivers have built in codes to subtract out the ionospheric contribution in signal delay for Navigation

purposes but these are only applicable for mid latitude conditions and severely underestimate the ionospheric effects at low latitudes. With the advent of the GAIM model, low-latitude ionospheric specification in real time will significantly enhance GPS navigation capabilities by providing single frequency "error maps" to account for the real-time state of the low-latitude ionosphere. For Communication customers the large enhancements in peak electron densities on either side of the magnetic equator significantly affect radio frequency (RF) signals passing through the ionosphere and ground-to-ground high-frequency (HF) communication systems. This is especially pronounced under storm time ionospheric disturbance conditions [*Daglis et al.*, 2004].

References

Anderson, D. N., J. A. Klobuchar, P. H. Doherty, and R. G. Rastogi (1992), A comparison of theoretical modeling of the low latitude ionosphere against TEC data from the Indian longitudes during solar minimum, paper presented at International Beacon Symposium, Mass. Inst. of Technol., Boston, Mass.

Anderson, D. N., A. Anghel, K. Yumoto, M. Ishitsuka, and E. Kudeki (2002), Estimating daytime vertical E × B drift velocities in the equatorial *F*-region using ground-based magnetometer observations, *Geophys. Res. Lett.*, *29*(12), 1596, doi:10.1029/2001GL014562.

Balsley, B. B. (1964), Evidence of a stratified echoing region at 150 kilometers in the vicinity of the magnetic equator during daylight hours, *J. Geophys. Res.*, *69*, 1925.

Blanc, E., B. Mercandalli, and E. Houngninou (1996), Kilometric irregularities in the *E* and *F* regions of the daytime equatorial ionosphere observed by a high resolution HF radar, *Geophys. Res. Lett.*, *23*, 645.

Chau, J. L. (1998), Examination of various techniques for measuring wind velocities using clear-air radars, with emphasis on vertical wind measurements, Ph.D. thesis, Univ. of Colo., Boulder.

Daglis, I., D. Baker, J. Kappenman, M. Panasyuk, and E. Daly (2004), Effects of space weather on technology infrastructure, *Space Weather*, *2*, S02004, doi:10.1029/2003SW000044.

Fejer, B. G., and L. Scherliess (1995), Time dependent response of equatorial ionospheric electric fields to magnetospheric disturbances, *Geophys. Res. Lett.*, *22*, 851.

Haykin, S. (1994), *Neural Networks: A Comprehensive Foundation*, Macmillan, Old Tappan, N. J.

Hysell, D. L., and J. D. Burcham (1998), JULIA radar studies of equatorial spread *F*, *J. Geophys. Res.*, *103*, 29,155.

Hysell, D. L., and J. D. Burcham (2000), Ionospheric electric field estimates from radar observations of the equatorial electrojet, *J. Geophys. Res.*, *105*, 2443.

Hysell, D. L., M. F. Larsen, and R. F. Woodman (1997), JULIA radar studies of electric fields in the equatorial electrojet, *Geophys. Res. Lett.*, *24*, 1687.

Kelley, M. C., J. J. Makela, J. L. Chau, and M. J. Nicolls (2003), Penetration of the solar wind electric field into the magnetosphere/ionosphere system, *Geophys. Res. Lett.*, *30*(4), 1158, doi:10.1029/2002GL016321.

Kudeki, E., and C. Fawcett (1993), High resolution observations of 150 km echoes at Jicamarca, *Geophys. Res. Lett.*, *20*, 1987.

Kudeki, E., C. D. Fawcett, W. L. Ecklund, P. E. Johnston, and S. J. Franke (1998), Equatorial 150-km irregularities observed at Pohnpei, *Geophys. Res. Lett.*, *25*, 4079.

Masters, T. (1993), *Practical Neural Network Recipes in C++*, Academic, San Diego, Calif.

Moore, D. S., and G. P. McCabe (1993), *Introduction to the Practice of Statistics*, W. H. Freeman, New York.

Peymirat, C., A. D. Richmond, and A. T. Kobea (2000), Electrodynamic coupling of high and low latitudes: Simulations of shielding/over shielding effects, *J. Geophys. Res.*, *105*, 22,991.

Rastogi, R. G., and J. A. Klobuchar (1990), Ionospheric electron content within the equatorial F2 layer anomaly belt, *J. Geophys. Res.*, *95*, 19,045.

Reddy, C. A. (1989), The equatorial electrojet, *Pure Appl. Geophys.*, *131*, 485.

Richmond, A. D. (1973), Equatorial electrojet: I. Development of a model including winds and instabilities, *J. Atmos. Terr. Phys.*, *35*, 1082.

Richmond, A. D. (1989), Modeling the ionospheric wind dynamo: A review, *Pure Appl. Geophys.*, *131*, 413.

Scherliess, L., and B. G. Fejer (1999), Radar and satellite global equatorial *F* region vertical drift model, *J. Geophys. Res.*, *104*, 6829.

Schunk, R. W., et al. (2004), Global Assimilation of Ionospheric Measurements (GAIM), *Radio Sci.*, *39*, RS1S02, doi:10.1029/2002RS002794.

Spiro, R. W., R. A. Wolf, and B. G. Fejer (1988), Penetration of high-latitude-electric-field effects to low latitudes during SUNDIAL 1984, *Ann. Geophys.*, *6*, 39.

Tsunoda, R. T., and W. L. Ecklund (2000), On the nature of 150-km radar echoes over the magnetic dip equator, *Geophys. Res. Lett.*, *27*, 657.

Woodman, R. F., and F. Villanueva (1995), Comparisons of electric fields measured at *F*-region heights with 150 km−irregularity drift measurements, paper presented at the Ninth International Symposium on Equatorial Aeronomy, Natl. Sci. Found., Bali, Indonesia.

————————
D. Anderson and A. Anghel, Space Environment Center, NOAA, 325 Broadway, Boulder, CO 80303, USA. (david.anderson@noaa.gov)

J. Chau and O. Veliz, Radio Observatorio de Jicamarca, Instituto Geofisico del Peru, Apartado 13-0206 Lima, Peru 13.